

Phonon Sidebands in the Emission Spectrum of O_2^- in Alkali-Halide Crystals

John Rolfe and M. Ikezawa*

Radio Division, National Research Council, Ottawa, K1A 0R8, Canada

T. Timusk

Laboratory of Atomic and Solid State Physics, Cornell University, Ithaca, New York 14850†

(Received 9 October 1972)

The emission spectra of O_2^- ions dissolved in alkali-halide crystals consist of a series of zero-phonon lines each accompanied by multiphonon sidebands. We present high-resolution measurements of such emission spectra at 2 °K in the alkali halides NaCl, KCl, KBr, KI, RbCl, RbBr, and RbI. The zero-phonon lines are due to vibronic transitions within the O_2^- molecule, and the sidebands are produced by the interaction of even-parity lattice modes with the allowed $\Pi_g \leftarrow \Pi_u$ transition corresponding to the O_2^- emission. We show that most of the sideband structure can be explained by coupling with A_{1g} lattice modes perturbed by relatively small changes in nearest-neighbor force constants. In two cases (KCl and RbCl) it is necessary to add T_{2g} modes, or to consider changes in other force constants, to obtain better agreement between calculated and observed sidebands. A residual spectrum at very low frequencies cannot be explained by the above hypothesis; it is assigned to a second-order coupling to librations of the O_2^- ion. Some broad features in the emission spectra are interpreted in terms of transitions to short-lived low-lying electronic states.

I. INTRODUCTION

The O_2^- ion in solid solution in alkali-halide crystals was first identified by paramagnetic-resonance measurements.¹ The yellow luminescence associated with O_2^- has been known for many years²; it was first identified as being due to O_2^- by Rolfe *et al.*³

The luminescence is due to a ${}^2\Pi_g \leftarrow {}^2\Pi_u$ electronic transition, as was first shown by Zeller and Känzig⁴ by measurement of the polarized absorption caused by uniaxial stress, and confirmed by Ikezawa and Rolfe⁵ by measurement of the effect of uniaxial stress on the emission spectra. These measurements show that the transition dipole of the emission transition lies parallel to the molecular axis of O_2^- ; that the axis is parallel to $\langle 110 \rangle$ directions in KCl, RbCl, RbBr, and RbI, but that the axis is parallel to $\langle 111 \rangle$ directions in NaCl, KBr, and KI.

The emission spectrum of O_2^- consists of a number of zero-phonon lines separated by approximately 1000 cm^{-1} . This frequency corresponds to the separation of the vibrational energy levels of the O_2^- ion in the ground state. The spectroscopic constants of this emission transition, at 2 °K, vary with the alkali-halide host lattice, the approximate values being $\nu_{00} = 27\,000\text{ cm}^{-1}$, $\omega_0'' = 1130\text{ cm}^{-1}$, and $\omega_0'' x_0'' = 9\text{ cm}^{-1}$. In this paper we will be entirely concerned with the multiphonon sidebands that lie on the low-energy side of the zero-phonon lines.

The most recent sideband spectra of O_2^- have been published by Rebane and Saari^{6,7} for the alkali halides NaCl, NaBr, KCl, KBr, KI, RbCl, and RbBr. Our sideband spectra reveal more de-

tail, mainly because we have a higher signal-to-noise ratio. Rebane and co-workers^{7,8} have also measured the half-widths of some O_2^- zero-phonon lines, and have calculated some coupling coefficients of the zero-phonon transitions with the lattice. Our results are in very good agreement with theirs.

II. APPARATUS

The same apparatus was used as described in the earlier paper.⁵ All of the spectra reported here are unaffected by the resolving power of the detection monochromator. This was proved by measuring the spectra again with smaller band-pass, when identical spectra resulted. All observations were taken at 1.96 °K, calculated from the equilibrium vapor pressure above the liquid helium in which the specimens immersed.

Crystal specimens were cleaved from boules grown in an oxygen atmosphere from melts containing approximately 0.5-wt% KO_2 , potassium superoxide. This method of preparation was found to give the highest concentration of O_2^- in the crystals.

III. RESULTS: GENERAL FEATURES OF EMISSION SPECTRA

The emission of O_2^- in NaCl is plotted in Fig. 1 using a logarithmic scale of intensity so that strong and weak components of the spectrum can both be shown clearly. The zero-phonon lines of the ${}^{16}O_2^-$ molecule are the most intense features present. These are labeled with the quantum number v'' of the ground state of the O_2^- ion; all the transitions originate from the $v' = 0$ level of the excited

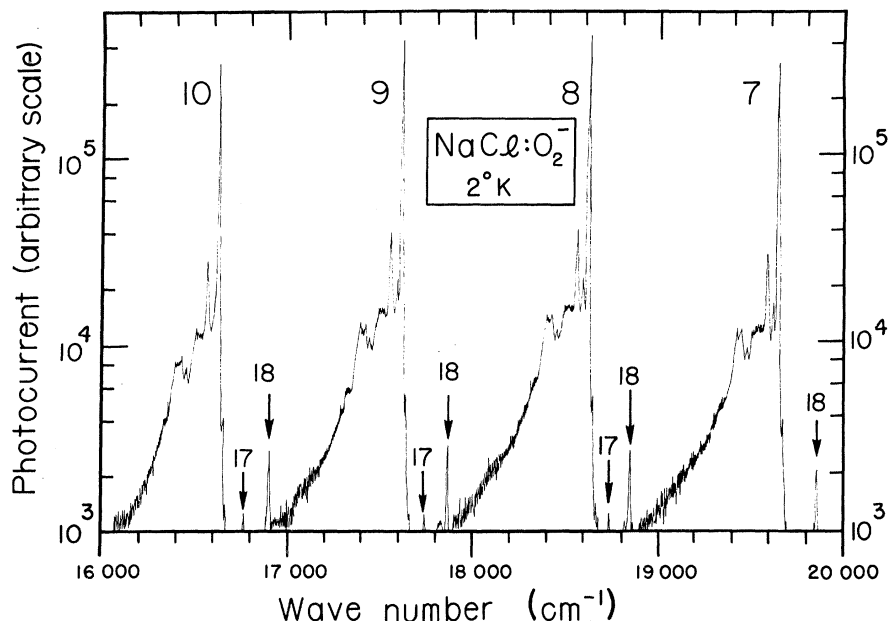


FIG. 1. Part of the emission spectrum of $\text{NaCl}:\text{O}_2^-$ plotted on a logarithmic photocurrent scale vs wave number. Upper numbers are the vibrational quantum numbers v'' of the $^{16}\text{O}_2^-$ molecule; lines labeled 17 and 18 are zero-phonon lines of the isotopic molecules $^{18}\text{O}^{16}\text{O}^-$ and $^{17}\text{O}^{16}\text{O}^-$.

state because of the very low temperature of the crystal. The small zero-phonon lines labeled "17" and "18" correspond to transitions of the isotopic molecular species $^{17}\text{O}^{16}\text{O}^-$ and $^{18}\text{O}^{16}\text{O}^-$, with natural abundances 0.07 and 0.4%, respectively. Multiphonon sidebands of $^{16}\text{O}_2^-$ are clearly visible in Fig. 1, to the low-energy side of the zero-phonon lines. The zero-phonon lines of the isotopic molecules are so small that their multiphonon sidebands are unobservable.

The phonon sidebands in Fig. 1 change very little in shape with quantum number v'' . This is generally true for the other alkali halides also; the only change with quantum number is a decrease of the sideband intensity relative to the zero-phonon line as the quantum number increases.

In Figs. 2-7, the 0-9 zero-phonon lines of O_2^- in six other alkali halides are shown, together with surrounding details, on a logarithmic intensity scale. Some features occur in these spectra which were not present in the $\text{NaCl}:\text{O}_2^-$ spectrum (Fig. 1). The largest extra feature appears in Fig. 2, in $\text{KCl}:\text{O}_2^-$. A complete broad extra feature occurs almost midway between adjacent zero-phonon lines. It is almost certain that this is intrinsic to the O_2^- emission spectrum in KCl, because we found that the intensity of this extra feature relative to the zero-phonon line could not be changed by adding extra impurities, by changing the O_2^- concentration, by changing the temperature, or by application of uniaxial stress.

Broad features also occur in the rubidium halides, which, though of low intensity, can be seen very clearly in the logarithmic spectra of Figs. 5-7. In $\text{RbCl}:\text{O}_2^-$ the broad band is situated right

under the normal (zero-phonon plus multiphonon) spectrum, in $\text{RbBr}:\text{O}_2^-$ the peak of the broad band is about 180 cm^{-1} on the high-energy side of the zero-phonon line, and in $\text{RbI}:\text{O}_2^-$ the peak is about 270 cm^{-1} away from the zero-phonon line in the same direction. Again it can be assumed that the broad band is an intrinsic part of the O_2^- emission

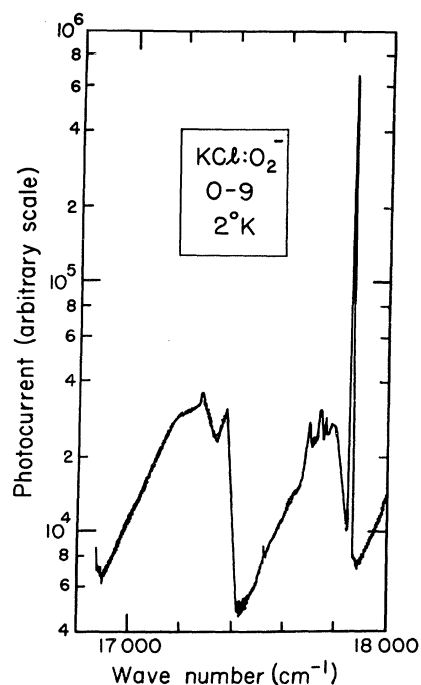


FIG. 2. Part of the emission spectrum of $\text{KCl}:\text{O}_2^-$, with $v''=9$ $^{16}\text{O}_2^-$ zero-phonon line and associated sidebands.

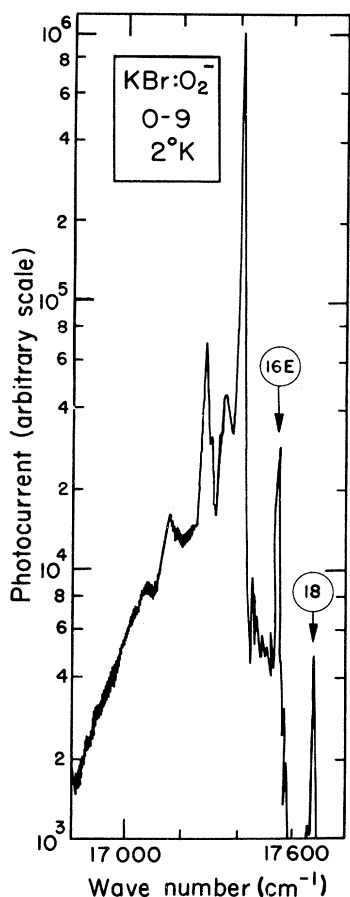


FIG. 3. Part of the emission spectrum of $\text{KBr}:\text{O}_2^-$ showing $v''=9$ $^{16}\text{O}_2^-$ extra zero-phonon line (marked 16E) and $^{18}\text{O}^{16}\text{O}^-$ isotope zero-phonon line (marked 18).

spectrum in the rubidium halides, because it showed a complete insensitivity to changes in impurity concentration and external stresses.

Finally, in $\text{KBr}:\text{O}_2^-$ (Fig. 3) a small zero-phonon line, labeled 16E in the diagram appears at about 130 cm^{-1} to the high-energy side of the larger zero-phonon line. This is called the "extra" zero-phonon line, and we have shown⁵ that the transition dipole giving rise to this emission lies in a $\{100\}$ plane, in contrast to the $\langle 111 \rangle$ dipole of the ordinary zero-phonon line. This extra line is intense enough to have an observable multiphonon sideband associated with it, whose frequency distribution is certainly different from the multiphonon sideband associated with the ordinary zero-phonon line. However, most of the sideband is obscured by the superimposition of the large ordinary zero-phonon line and its associated sideband, so that the sideband of the extra zero-phonon line cannot be accurately measured.

Fortunately, the extra features discussed above interfere very little with the main multiphonon

sidebands that we are interested in here. In $\text{KCl}:\text{O}_2^-$ the extra feature is well removed in frequency from the main sideband region, and in KBr and the rubidium halides the extra features have negligible intensities in the main phonon sideband region. In NaCl and KI no extra features appear.

In Sec. IV we will discuss the origin and the frequency spectra of the main phonon sidebands. After this has been done we will speculate on the origin of the broad extra features described above.

IV. THEORY OF PHONON SIDEBANDS

A. General

Several mechanisms can give rise to phonon sidebands of a high-frequency transition. It is helpful to distinguish between sidebands of forbid-

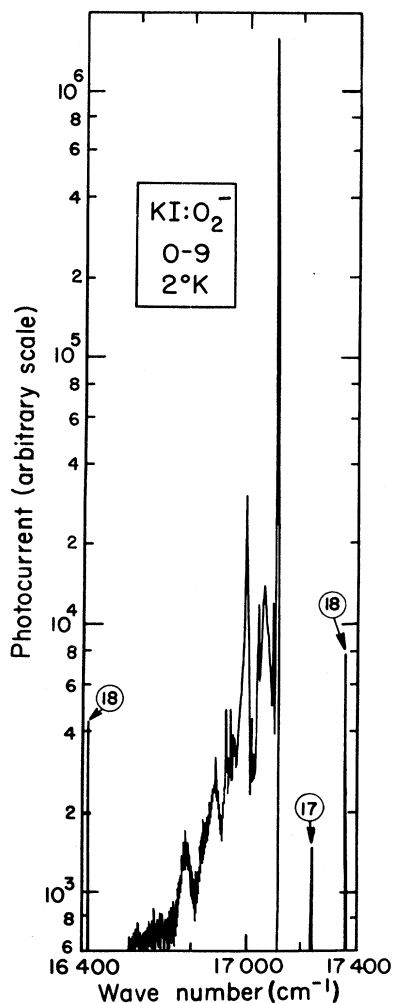


FIG. 4. Part of the emission spectrum of $\text{KI}:\text{O}_2^-$ showing the $v''=9$ $^{16}\text{O}_2^-$ zero-phonon line, the two $v''=9$ isotopic $^{17}\text{O}^{16}\text{O}^-$ and $^{18}\text{O}^{16}\text{O}^-$ zero-phonon lines belonging to $v''=9$ on the right-hand side, and an $^{18}\text{O}^{16}\text{O}^-$ zero-phonon line belonging to $v''=10$, on the left-hand side.

den and allowed transitions. Forbidden transitions can be made allowed by absorption or emission of a phonon; a sideband is produced in this way and in general it will reflect some odd-parity projection of the phonon density of states. The parent zero-phonon line is either absent or very faint due to weak magnetic-dipole or defect induced electric-dipole processes and multiphonon sidebands are absent. The one-phonon sideband strength is calculated by straightforward second-order perturbation theory. Allowed transitions, on the other hand, such as the $\Pi_u - \Pi_g$ fluorescence of O_2^- discussed here, often exhibit strong multiphonon sidebands corresponding to even-parity phonons. These sidebands arise from transitions between harmonic oscillator states of the phonons with displaced equilibrium positions. A characteristic of this Frank-Condon or overlap mechanism is that the relative intensities of all the multiphonon lines of a given mode are given by the simple Poisson distribution. A parallel formal development of the two mechanisms is given by Bron.⁹ In this paper we are only concerned with the second mechanism.

The sidebands due to the overlap mechanism are usually discussed in terms of a "molecular" approximation where one assumes only a few modes

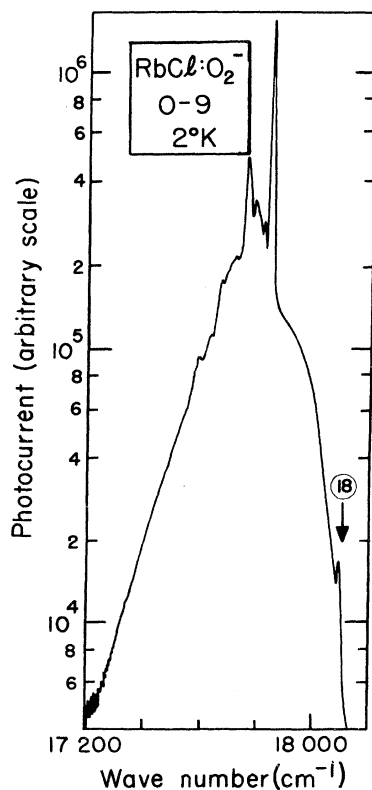


FIG. 5. Part of the emission spectrum of $RbCl:O_2^-$ showing the $^{16}O_2^-$ zero-phonon line and the $^{18}O_2^-$ zero-phonon line both belonging to $v''=9$.

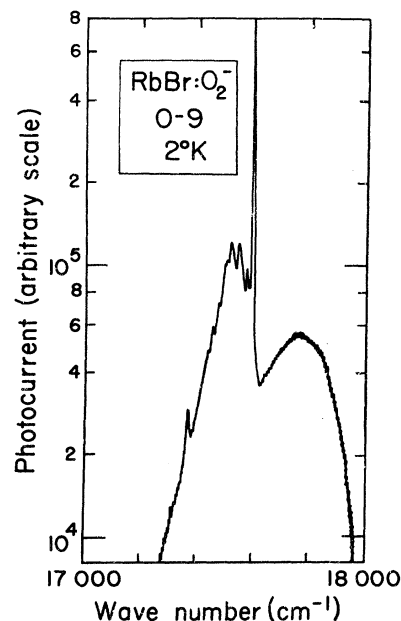


FIG. 6. Part of the emission spectrum of $RbBr:O_2^-$ showing the $v''=9$ $^{16}O_2^-$ zero-phonon line. No isotope zero-phonon lines are visible.

interact with the transition. This restriction is not necessary, however, and we will follow here a slightly modified previous treatment¹⁰ used in describing the sidebands of the H^- -ion local mode in the alkali halides.

We start by expanding the adiabatic potential of

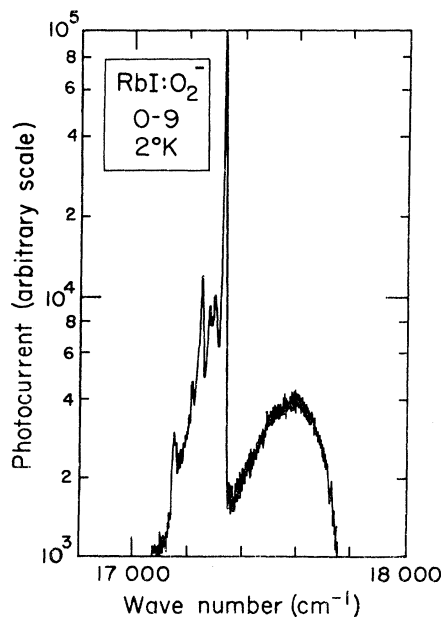


FIG. 7. Part of the emission spectrum of $RbI:O_2^-$ showing the $v''=9$ $^{16}O_2^-$ zero-phonon line. No isotope zero-phonon lines are visible.

the crystal in the Born–Oppenheimer approximation in coordinates Q_i which transform according to some row of an irreducible representation of the symmetry group of the Hamiltonian centered on the impurity ion. One of the Q_i 's, for example, is the totally symmetric breathing motion of the nearest neighbors. It should be noted, however, that the Q_i are not the normal modes of the system; each Q_i is associated with a continuous spectrum up to the highest frequency of the crystal. Only when by a suitably large change of force constants one of the Q_i becomes a local mode will it be an eigenmode with a sharp frequency. The initial state for the fluorescence process is the lowest vibrational level of the excited electronic state and we expand its adiabatic potential in Q_i :

$$E_e = E_0 + \frac{1}{2} \sum_{ij} \frac{\partial^2 E_e}{\partial Q_i \partial Q_j} Q_i Q_j + \dots, \quad (1)$$

where E_0 is the zero-phonon–line energy and where we have chosen the equilibrium position of Q_i in such a way as to make the term linear in Q_i vanish. This term does not vanish in the ground state, and we have

$$E_g = \sum_i \frac{\partial E_g}{\partial Q_i} Q_i + \frac{1}{2} \sum_{ij} \frac{\partial^2 E_g}{\partial Q_i \partial Q_j} Q_i Q_j + \dots \quad (2)$$

We are mainly interested in one-phonon sidebands and it has been shown by Maradudin¹¹ in a very general way that the quadratic terms make no contribution to the one-phonon spectrum. We therefore neglect changes of the second-order term and assume it is the same in the excited and ground states.

In order to make use of results applicable to displaced harmonic-oscillator wave functions we expand the Q_i in terms of the true normal modes q_i of the crystal with the impurity:

$$Q_i = \sum_l \langle Q_i | l \rangle q_l, \quad (3)$$

where the q_l obey a harmonic-oscillator Hamiltonian

$$H = \frac{1}{2} p_l^2 + \frac{1}{2} \omega_l^2 q_l^2.$$

The ground-state energy after the transition but before relaxation of the lattice to a new equilibrium position, in terms of the Q_i , is given by

$$E_g(0) = \sum_i \sum_l \frac{\partial E_g}{\partial Q_i} \langle Q_i | l \rangle q_l = \sum_i \frac{1}{2} \omega_i^2 q_{0i}^2, \quad (4)$$

where q_{0i} is the shift of the equilibrium position of coordinate q_i . This energy is a measure of the strength of the coupling of the transition to the mode q_i and it is most conveniently discussed in terms of the dimensionless parameter S_i , defined as

$$S_i \equiv \omega_i^2 q_{0i}^2 / 2\hbar \omega_i. \quad (5)$$

From (4) we find that the frequency distribution of S_i , defined as

$$S(\omega) \equiv \sum_i \left(\frac{\omega}{2\hbar} \right) q_{0i}^2 \delta(\omega_i - \omega), \quad (6)$$

is given by

$$S(\omega) = \sum_{ij} \sum_l \left(\frac{2}{\hbar \omega^2} \right) \frac{\partial E_g}{\partial Q_i} \langle Q_i | l \rangle \delta(\omega_i^2 - \omega^2) \times \langle l | Q_j \rangle \frac{\partial E_g}{\partial Q_j}. \quad (7)$$

We have expressed $S(\omega)$ in such a way that it contains the imaginary part of the Green's function of the perturbed crystal,

$$\lim_{\epsilon \rightarrow 0} G_{ij}(\omega + i\epsilon) = \sum_l \langle Q_i | l \rangle (\omega_i^2 - \omega^2 - i\epsilon)^{-1} \langle l | Q_j \rangle, \quad (8)$$

labeled by the irreducible representations of the group of the crystal centered on the impurity. This representation simplifies the calculation of G in terms of G_0 , the Green's function of the perfect crystal. If Γ is the matrix of force-constant changes, brought about by the defect, we have

$$G = G_0 [1 / (1 + \Gamma G_0)], \quad (9)$$

where the matrix inversion is made easier by the block-diagonal form of Γ .¹² Further, since G does not couple coordinates that belong to different irreducible representations or different rows of the same representation, the number of terms over i and j in Eq. (7) will be reduced.

The phonon sideband can now be calculated. The transition probability is proportional to an electronic-dipole matrix element multiplied by an overlap integral between the ground and excited states of the vibrational wave functions for each coordinate q_i .¹³ A single normal mode q_i of the perturbed crystal contributes a δ function of strength S_i to the one-phonon sideband at a frequency ω_i removed from the zero-phonon line. The two-phonon amplitude is $\frac{1}{2} S_i^2$ and appears at frequency $2\omega_i$. The n -phonon sideband can be obtained by calculating the n -fold convolution of the one-phonon sideband and multiplying the result by $S^n/n!$, where

$$S \equiv \int_0^\infty S(\omega) d\omega.$$

To simplify the discussion of the contribution of the various Q_i to the sideband we also introduce a mode $S_{ij}(\omega)$:

$$S_{ij}(\omega) \equiv \frac{\partial E_g}{\partial Q_i} G_{ij}(\omega) \frac{\partial E_g}{\partial Q_j}.$$

It will be seen that $S = \sum S_{ij}$. In most of our calculations the off-diagonal elements of S_{ij} are zero¹⁴ and we refer to the diagonal element with a single subscript, $S_i \equiv S_{ii}$. The quantities $\partial E_g / \partial Q_i$ act as

coupling coefficients of the transition to the symmetry coordinate i . It is useful to think of them as components of a vector, the gradient vector of the ground-state adiabatic potential expressed in terms of symmetry coordinates.

The unknown parameters in this problem are the components of this gradient vector $\partial Q_g/\partial E_i$, the elements of the force-constant-change matrix Γ , and the elements of G_0 (the Green's function of the perfect lattice). We use shell models derived from inelastic neutron scattering for G_0 but for Γ and $\partial E_g/\partial Q_i$ we have no accurate independent data. A calculation of these quantities from first principles is difficult so we will treat these quantities as adjustable parameters.

B. Model of O_2^- Defect

1. Perturbation Matrix Γ

The matrix Γ describes the changes in the force constants caused by the defect and has the symmetry of the crystal with the defect. In NaCl, KBr, and KI the molecular axis of O_2^- points along $\langle 111 \rangle$ directions in the excited state.⁵ If we further assume that O_2^- is centered on the lattice site, the point group of the defect is D_{3h} , the trigonal group. Similarly, the O_2^- axis in KCl, RbCl, RbBr, and RbI points along $\langle 110 \rangle$ directions and the point group is D_{2h} or orthorhombic. We have assumed in our development of the expressions for S that we can neglect changes in force constants of the system between excited and ground states. In terms of Γ this implies that we are assuming a common Γ for the excited state and the (unrelaxed) ground state. Figure 8 shows the force-constant models we have examined in the two cases. In the figure the various symbols joining the atomic positions refer to the force constants that have been changed from their pure lattice values. In the trigonal case the force-constant-change matrix Γ is

$$\Gamma = \frac{1}{2} \begin{pmatrix} \Delta f & 0 & 0 \\ 0 & \Delta f & 0 \\ 0 & 0 & \Delta t \end{pmatrix} \begin{matrix} A_{1g} \\ E_g \\ T_{2g} \end{matrix},$$

where the rows and columns are labeled by the Q_i that transform according to irreducible representations of the O_h group. In the trigonal group (D_{3h}) these representations are all of A_{1g} symmetry. In this matrix Δf is the nearest neighbor to impurity force constant and Δt is a trigonally symmetric linear combination of first-neighbor to second-neighbor force constants, which gives the restoring force for the $(1/\sqrt{3})(T_{yz} + T_{zx} + T_{xy})$ T_{2g} mode (Fig. 9) of the nearest neighbors. These force-constant changes are illustrated in Fig. 8(a).

In the orthorhombic case (D_{2h}), the Γ matrix is

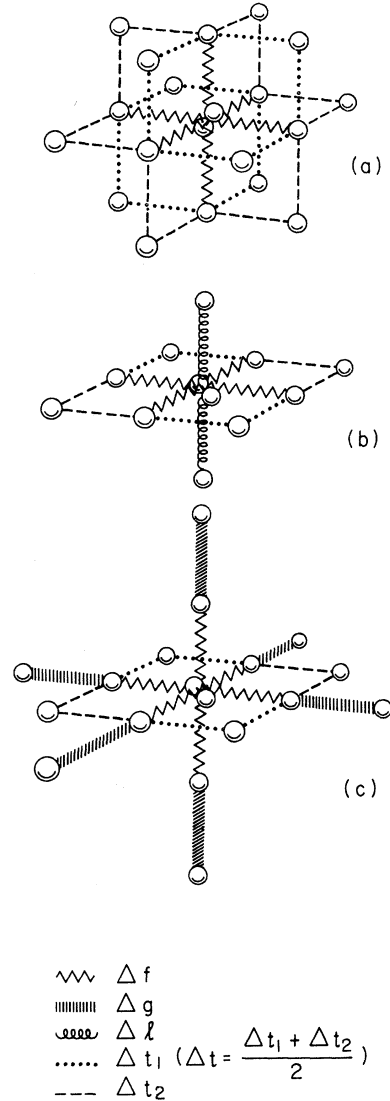


FIG. 8. Location of the force-constant changes around the O_2^- impurity. The key at the bottom of the figure identifies the symbols used in force-constant-change matrices Γ . Model (a) was used for the trigonal O_2^- centers, model (b) for the orthorhombic centers, except in KCl, and model (c) was used for O_2^- in KCl.

$$\Gamma = \frac{1}{2} \begin{pmatrix} \Delta f + \Delta l & \Delta f - \Delta l & 0 \\ \Delta f - \Delta l & \Delta f + \Delta l & 0 \\ 0 & 0 & 2\Delta t \end{pmatrix} \begin{matrix} A_{1g} \\ E_g \\ T_{2g} \end{matrix}.$$

There are two generally different force constants Δf and Δl that connect the defect to its nearest neighbors. We have again made use of a force constant Δt that acts as a restoring force on the T_{2g} vibration that transforms as A_{1g} in D_{2h} [Fig. 9(b)]. These force-constant changes are shown in Fig. 8(b). In KCl we have also made use of a more

complex Γ matrix incorporating the first-neighbor to fourth-neighbor force-constant change Δg to account for relaxation¹⁵ [see Fig. 8(c)].

As mentioned earlier, the "extra line" in KBr arises from O_2^- molecules which are probably oriented along $\langle 100 \rangle$, implying a distortion of D_4 symmetry.⁵ Such distortions would be described by a matrix similar to the orthorhombic Γ matrix, but without the T_{2g} mode.

It is clear that the force-constant models we have chosen are simplifications. We have treated the O_2^- molecule as a point mass connected by arbitrary radial force constants to the nearest neighbors. The tangential force constants, second-neighbor force constants, and the Coulomb forces are all assumed to be the same as those of the corresponding ion in the unperturbed lattice. We can justify this simplification as follows. First, the tangential, second-neighbor, and Coulomb force constants in the host crystal are roughly an order of magnitude smaller than the radial repulsive force constants.¹⁶ Second, our results will show that the changes in the important nearest-neighbor force constants themselves are relatively small in most cases and support a view of the O_2^- as a mildly perturbing defect in most of the alkali halides. The neglect of the internal structure of O_2^- , the stretching and libration degrees of freedom, can also be justified. The internal stretching mode has such a high frequency that it is effectively decoupled from the lattice. The librations of the O_2^- are not totally symmetric and do not affect the even-symmetry modes under study. This does not mean that they cannot couple in second order to produce a sideband, and to calculate the spectrum of these modes we must use models for Γ that take into account the nonradial coupling of the neighbors to the defect.

2. Modes of Nearest Neighbors that Interact with Transition

The $\Pi_u \rightarrow \Pi_g$ transition is an allowed transition polarized along the direction of the O_2^- molecular axis. According to the selection rules first enunciated by Herzberg and Teller,¹⁷ modes that interact with an allowed transition are those that are totally symmetric in the lower symmetry state of the two states Π_u and Π_g of the molecule.¹⁸ Since the final relaxed ground state is always of D_{2h} symmetry we should include all totally symmetric modes in D_{2h} of the nearest neighbors for both $\langle 110 \rangle$ -oriented centers as well as the $\langle 111 \rangle$ centers. The nearest-neighbor modes of even symmetry that develop into A_1 modes of D_{2h} are the A_{1g} , E_g , and T_{2g} modes of the O_h group. Thus if we assume that the system relaxes towards a configuration that has inversion symmetry and is at least orthorhombic we need only consider A_{1g} , E_g , and T_{2g} modes of the nearest neighbors. Figure 9

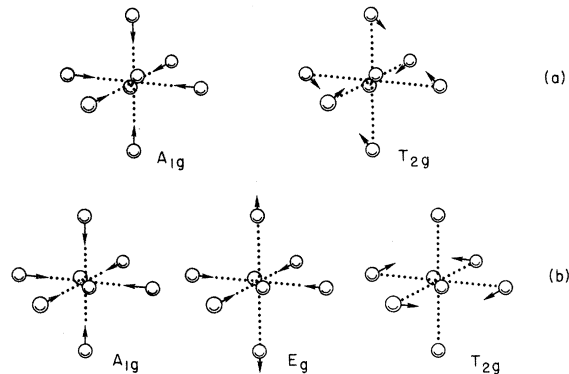


FIG. 9. Classification of nearest-neighbor vibrational modes of (a) trigonal O_2^- ions, and (b) orthorhombic O_2^- ions.

shows the displacements of the nearest neighbors for the modes we have examined.

3. Librations of O_2^-

There are only three A_1 modes in D_{2h} of the nearest neighbors. Other modes that are relevant are the stretching of O_2^- which couples strongly to the transition and has been discussed previously.⁵ We would also like to consider nontotally symmetric motions which can couple to the transition in second order. Of these, librations of O_2^- about its molecular axis would be particularly important because of the large amplitude of librational motion occurring in a region of low-phonon density of states. One mechanism for librational coupling is through the second-order terms in vibrational overlap in Eqs. (1) and (2). If the librational frequency is markedly different in ground and excited states, the sideband contribution from this process can be quite large. Kiel¹⁹ has calculated an equivalent S for this process, and he finds

$$S = (\omega_a - \omega_b) / (\omega_a + \omega_b),$$

where ω_a and ω_b are ground- and excited-state frequencies. In terms of this quantity the l th libration sideband has a strength

$$I_l = I_0 \frac{2^l}{2^{2l}(l!)} S^{2l},$$

where I_0 is the zero-phonon line strength. We suggest that some of the low-frequency structure that cannot be explained in terms of the nearest-neighbor motions may be due to librational coupling by this mechanism.

V. CALCULATION OF SIDEBAND SPECTRA

The details of the calculation of sideband spectra have been given in previous publications.^{10,15} We used the Cochran-Cowley shell model¹⁶ with parameters determined from inelastic-neutron-

scattering experiments, using the sources quoted in Table I. We calculated a set of 1686 independent wave vectors in the Brillouin zone for the phonons, sorting the contributions into frequency intervals 0.5 cm^{-1} wide, except for NaCl where 1.0 cm^{-1} intervals were used.

These calculated one-phonon sidebands were then successively convoluted to produce two-, three-, and four-phonon sidebands, which were then added together in the proportions required by the value of the coupling constant S . Contributions from the five-phonon and higher sidebands were completely negligible for the small values of the coupling constant used here.

The calculated multiphonon sidebands may contain detail finer than what can be observed experimentally; so the multiphonon sideband was convoluted once again, this time with a broadening function, arbitrarily chosen as triangular, whose half-width could be varied. The parameters used in the best fits between theory and experiment are listed in Table I.

In carrying out our adjustment of the parameters of the models we tried at all times to keep the number of parameters small. Thus if the introduction of a new parameter resulted in only a slight improvement of the calculated spectrum, it was discarded. In general we had available to us up to three force-constant changes and three coupling constants for different modes. In most cases, however, we were able to obtain a good fit with experiment by using only one force-constant change and one coupling constant. The method of

adjusting the parameters was as follows: First, the unperturbed eigenmodes were used to calculate the frequency spectra of the A_{1g} nearest-neighbor motions, and then the nearest-neighbor radial force-constant changes Δf were allowed to vary, with $\Delta f = \Delta l$ for the orthorhombic case. Quite good agreement between theory and experiment was obtained by making this single adjustment for NaCl, KBr, KI, RbBr, and RbI, as shown in Table I. It should be noted that in all calculations for orthorhombic centers the effect of orthorhombic distortion was examined by varying Δl independently of Δf . However, the spectra proved relatively insensitive to changes of Δl , so that orthorhombic distortion was not used in the final best fits to experiment.

For the two remaining alkali halides, KCl and RbCl, it was found necessary to adjust more than one parameter. In both of these it was necessary to add unperturbed ($\Delta t = 0$) T_{2g} modes to the A_{1g} modes to attain better agreement with experiment in the low-frequency region, and in the case of KCl it was necessary to change the first- to fourth-neighbor force constant by an amount Δg .

The T_{2g} modes are concentrated in the low-frequency part of the spectrum, and we found that large changes in force constant Δt were required to cause an appreciable shift of the low-frequency modes. If any of the low-frequency peaks that we assign to librations are to be ascribed to an admixture of T_{2g} modes to the basic A_{1g} spectrum, then the force-constant changes Δt which would be necessary are much larger than the changes Δf .

TABLE I. Parameters used in calculating sidebands, and some experimental data.

Crystal	Symmetry	Phonon-data reference	Δf (dyn cm^{-1})	Δg (dyn cm^{-1})	$S_{A_{1g}}$	$S_{T_{2g}}$	Broadening width (cm^{-1})	Experimental data $\nu'' = 9$ FWHM (cm^{-1})	S
NaCl	D_{3h}	a	1000	0	1.3	0	8	5.0	...
KCl	D_{2h}	b	2000	4000	0.75 0.97	0.65 0.43	7	2.5	...
KBr	D_{3h}	c	-5500	0	1.0	0	3.5	2.2 ^d	0.5
KI	D_{3h}	e	-8000	0	0.9	0	1	1.0	0.4
RbCl	D_{2h}	f	0	0	1.5 0.78	0 0.73	14	7.0	...
RbBr	D_{2h}	g	-4000	0	1.3	0	6	5.0	...
RbI	D_{2h}	h	-2000	0	1.2	0	5	3.9	...

^aG. Raunio and S. Rolandson, Phys. Rev. B 2, 2098 (1970), model 3.

^bReference a, model 2.

^cReference 16, model VI.

^d $\nu'' = 12$.

^eG. Dolling, R. A. Cowley, C. Schittenhelm, and I. M.

Thorson, Phys. Rev. 147, 577 (1966), model III.

^fReference a, model 2.

^gS. Rolandson and G. Raunio, J. Phys. C 4, 958 (1971), model II.

^hG. Raunio and S. Rolandson, Phys. Status Solidi 40, 749 (1970), model 2.

Such a model is unreasonable on physical grounds since any relaxation around O_2^- would be certain to cause a much larger change Δf than Δt . Furthermore, when such large changes in force constant are made the peaks moved to low frequencies and developed into strong resonances, which contain nearly all the intensity of the spectrum. We are therefore led to conclude that the low-frequency peaks do not correspond to any of the motions of the six nearest neighbors of the O_2^- ion illustrated in Fig. 9. We will assume that peaks left unexplained by the nearest-neighbor model arise from librations of O_2^- about its equilibrium position and we will ignore these peaks in our fitting procedures which only involve nearest neighbors and radial force constants. Thus we have left $\Delta t=0$. The librational part of the emission spectra of O_2^- will be considered in detail in a later publication.

VI. COMPARISON OF CALCULATED AND OBSERVED SPECTRA

A. NaCl

Figure 10 shows the experimental curve for the fluorescence sideband of the 0-9 emission line at 2°K along with a calculated curve using $S_{A_{1g}} = 1.3$ and $\Delta f = 1000 \text{ dyn cm}^{-1}$. The force constant f itself in NaCl is $25700 \text{ dyn cm}^{-1}$. The small Δf was obtained by adjusting for a flat-top peak between 200 and 240 cm^{-1} . It will be seen that the structure above 120 cm^{-1} is quite well explained by nearest-neighbor breathing modes, but the strongest features of the spectrum, the peaks at 60 and 28 cm^{-1} along with a two-phonon contribution at 120 cm^{-1} , are not present in our model. Our conclusion is that in this case the coupling to the libration is very strong. If the librational-frequency change is large, the coupling to the libration is stronger and presumably in the small Cl^- cavity the O_2^- ro-

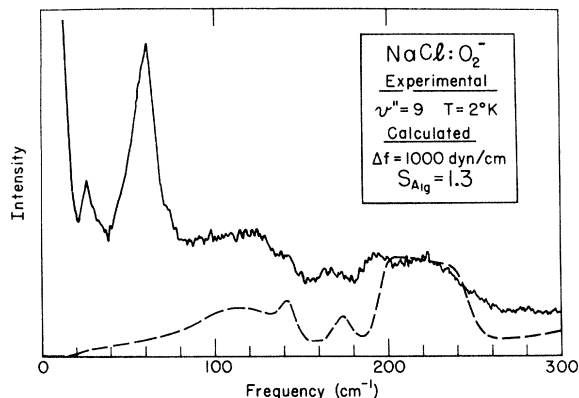


FIG. 10. Experimental and calculated sidebands of O_2^- in NaCl. The two largest low-frequency peaks are attributed to librations. In this and succeeding diagrams the solid line is the experimental spectrum.

tation is considerably hindered and, what is more important, changes strongly between excited and ground states.

B. KCl

Potassium chloride, shown in Fig. 11, is the spectrum most difficult to fit. The best combination of parameters we have been able to find is shown as the dashed curve on the figure. It uses modest increases of Δf and Δg along with an admixture of unperturbed T_{2g} modes. The fit is not too satisfactory, in particular, the peak at 120 cm^{-1} is too weak. Nearly all our models for KCl have this in common and it is at least partly explained by the two-phonon contribution of the 60-cm^{-1} structure which is also poorly represented by our models. The dotted curve uses a larger contribution of T_{2g} and raises the 60-cm^{-1} region slightly, but again we would prefer to assign the intensity here to libration in analogy with the other more unambiguous cases.

An independent test of the force-constant model for $KCl:O_2^-$ is obtained from recent impurity-induced far-infrared absorption measurements.²⁰ A reasonable fit to those experimental results is obtained by setting $\Delta f = -1000 \text{ dyn cm}^{-1}$ and $\Delta g = -500 \text{ dyn cm}^{-1}$ in contrast to the values $\Delta f = 2000 \text{ dyn cm}^{-1}$ and $\Delta g = 4000 \text{ dyn cm}^{-1}$, necessary here. The discrepancy between these models is larger than found in other systems and is an indication that the KCl model is unsatisfactory.

C. KBr

The larger space available for O_2^- in the KBr lattice leads one to expect a greater reduction of nearest-neighbor force constants, and we obtain quite good agreement with experiment (see Fig. 12) with $S_{A_{1g}} = 1.0$ and $\Delta f = -5500 \text{ dyn cm}^{-1}$, in good agreement with the parameters necessary to explain far-infrared absorption in $KBr:O_2^-$.¹⁷ The slight discrepancy in the position of the "step" at 70 cm^{-1} and the peak at 83 cm^{-1} is well understood from a study of other defects in KBr^{20,21}; it arises from an inaccuracy in the shell model for the phonons.

The zero-phonon line in $KBrO_2^-$ is anomalous. It is very broad at low quantum numbers (13 cm^{-1} at $\nu'' = 5$) and rapidly narrows as the quantum number increases, reaching a width of 2 cm^{-1} at $\nu'' = 12$. This fact was first noted by Rabane and Saar.²² The most intense sideband is at $\nu'' = 9$, but the zero-phonon linewidth is 4.4 cm^{-1} , so the less intense sideband at $\nu'' = 12$ was chosen for comparison with calculation because greater detail in the experimental sideband was judged more important than the increased noise. The broad zero-phonon line in KBr might imply some free rotorlike motions of the ion. Note the absence of

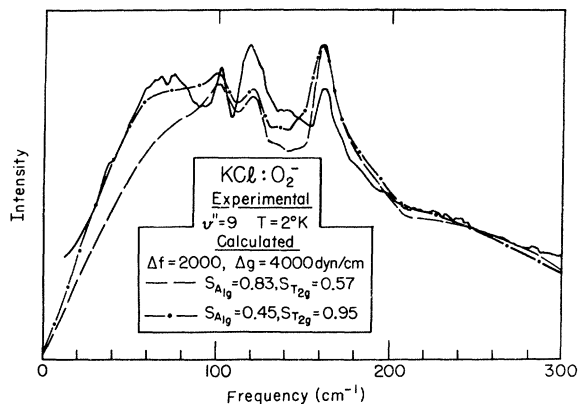


FIG. 11. Experimental and calculated sidebands of O_2^- in KCl, with varying amounts of coupling to T_{2g} modes.

strong unexplained peaks at low frequencies attributable to librations. However, at higher quantum numbers than $\nu''=12$ there are some sharp peaks at very low frequencies, for instance, a weak peak at 13 cm^{-1} .

The KBr sideband can be used to find the maximum possible contributions of E_g modes to the sideband, because of a large E_g singularity at 106 cm^{-1} , which does not appear in the experimental sideband. We can set an upper limit of $S_{E_g}=0.2$ by this method.

D. KI

In $KI:O_2^-$ we have the smallest coupling coefficient and the narrowest zero-phonon line, so that we have a large amount of detail present in the multiphonon sideband. Again a good fit to the experimental spectrum (see Fig. 13) can be obtained with the use of A_{1g} modes only and a change in the single force constant $\Delta f = -8000\text{ dyn cm}^{-1}$. This change is even larger than for KBr, in keeping

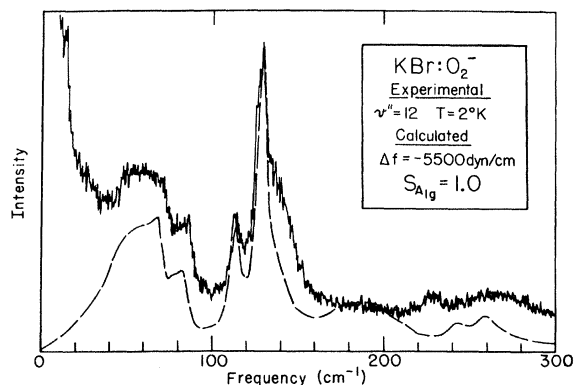


FIG. 12. Experimental and calculated sidebands of O_2^- in KBr. The coupling to librations is very weak in KBr.

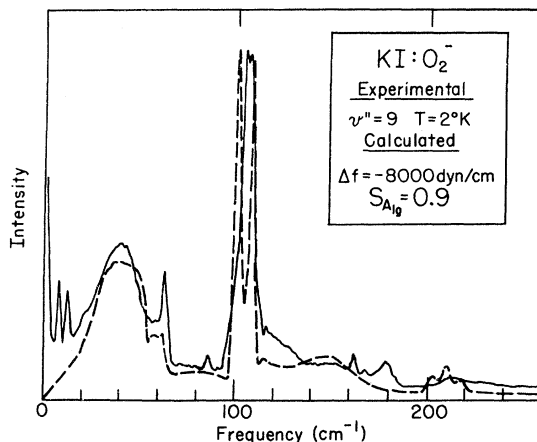


FIG. 13. Experimental and calculated sidebands of O_2^- in KI. Note the good agreement obtained with only one adjustable parameter.

with the larger lattice site available for the O_2^- . The force-constant change was fixed by the position and relative intensity of the two peaks in the 105-cm^{-1} region. Note the good agreement with the acoustical branch with this single parameter.

The two quite distinct sharp lines which appear at low frequencies, at 9 and 13 cm^{-1} , might be attributable to librations. There are some other unexplained small peaks in the system; a gap mode at 87 cm^{-1} , and two other peaks at 161 and 179 cm^{-1} . The 64-cm^{-1} acoustic-branch peak is too weak in the calculated spectrum, and also its two-phonon contribution at 116 cm^{-1} is underestimated. Note that the frequency of the peak is very accurately predicted, the experimental two-phonon peak being observed at 116 cm^{-1} and the calculated peak at 115 cm^{-1} . This peak arises from a singularity in the phonon density of states and is not affected by force-constant changes.

E. RbCl

The sideband of RbCl (Fig. 14) is best fitted by a zero force-constant change. The solid line shows the calculated sideband using A_{1g} modes only, but, as in the case of KCl, some improvement can be gained by introducing T_{2g} modes, when the intensity in the acoustic region is increased in agreement with experiment (see dotted line in Fig. 14), and also the intensity in the two-phonon region at 120 cm^{-1} is increased. The two peaks at 23 and 55 cm^{-1} cannot be fitted with T_{2g} modes and we would like to assign these to librations.

F. RbBr

Figure 15 shows the $0-9$ emission sideband of RbBr. Two strong lines attributable to librations can be seen at 18 and 43 cm^{-1} . The rest of the spectrum is reasonably well reproduced by A_{1g}

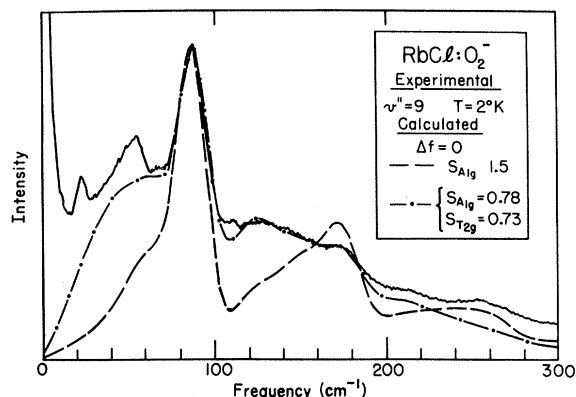


FIG. 14. Experimental and calculated sidebands of O_2^- in RbCl. Note that a zero force-constant change is used in the calculation, thus O_2^- in RbCl acts as an isotopic impurity.

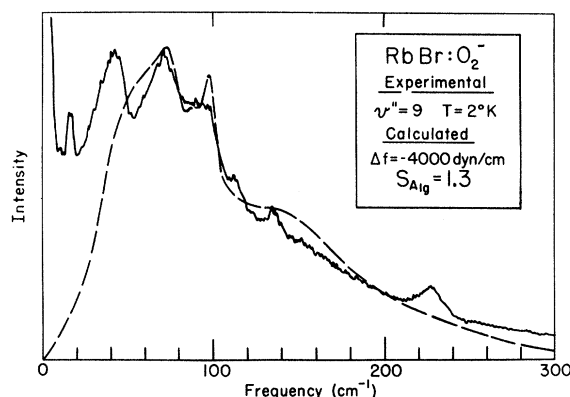


FIG. 15. Experimental and calculated sidebands of O_2^- in RbBr.

motions of nearest neighbors with a Δf of -4000 dyn cm^{-1} .

G. RbI

The RbI spectrum, shown in Fig. 16, is very similar to KBr, and again a modest change of force constant suffices to explain the spectrum with A_{1g} modes alone. We would again like to associate the peaks at 10 and 30 cm^{-1} with librations.

VIII. DISCUSSION

A. Broadening Functions and Coupling Constants

In calculating the sidebands that fitted the experimental data best, the broadening width and the coupling constant were regarded as freely adjustable parameters. In some cases the broadening width was found to be fairly well defined by the fitting procedures, for example, in RbI: O_2^- (Fig. 16) it was adjusted to get the correct width of the main peak at 75 cm^{-1} , and in KBr: O_2^- (Fig. 12) it was adjusted so that the subsidiary peak at 114 cm^{-1} was resolved to the same extent as in the experimental sideband. In other cases, such as KCl: O_2^- and NaCl: O_2^- , the precision with which the broadening width could be fixed was not nearly

so good. The coupling coefficient was adjusted to about the same degree of precision in all cases; the criterion was that the correct intensity be obtained in the two-phonon region.

These best-fit values of broadening width and coupling constant can be compared to values found by other methods. In the case of the broadening width, one would expect on the basis of the simple theory used that it would be equal to the measured half-width of the zero-phonon lines. The results of our measurement of the half-widths are collected together in Table II, and selected values from this table have been quoted in Table I. While it is true that the best-fit values of broadening width follow the same trend as the measured half-width, the best-fit values are always larger. The difference is greater than could be accounted for by the use of a triangular broadening function rather than a Gaussian or Lorentzian, and probably indicates that too simple a theory was used in the fitting procedure.

Similarly, there is an independent method of finding the coupling constant, from integrated intensities over the zero-phonon and multiphonon emission spectra. We first note that the change in the cube of the frequency over the 300- cm^{-1} range of the sidebands is only about 5% of the zero-phonon-line frequency. Within this error, therefore,

TABLE II. Full width at half-maximum of zero-phonon lines of O_2^- at 2 °K, in cm^{-1} .

ν''	3	4	5	6	7	8	9	10	11	12	13	14
NaCl	3.7	4.2	4.4	5.0	4.9	5.0
KCl	3.8	3.4	3.4	3.0	2.5	2.3	2.2	2.1	2.0	...
KBr	15.6	14.2	13.1	10.5	8.3	6.6	4.4	3.9	3.1	2.2	1.9	1.8
KI	1.12	1.00	1.05	1.02	1.06
RbCl	6.8	7.0	7.5
RbBr	6.2	6.1	5.8	5.7	5.0	5.0	4.8	4.6
RbI	5.0	4.6	4.7	4.3	3.9	3.6	3.7	3.3

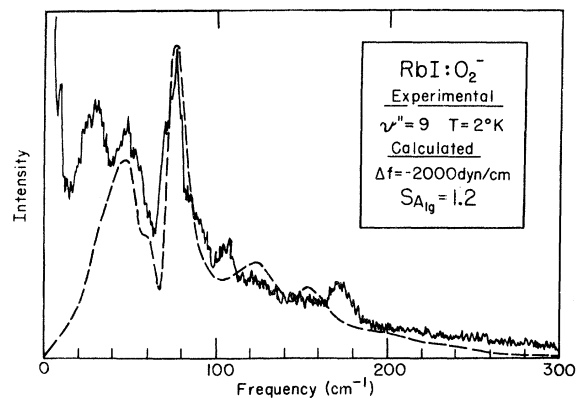


FIG. 16. Experimental and calculated sidebands of O_2^- in RbI.

the transition probability is proportional to the measured optical intensity, and thus the integrated emission intensity over the zero-phonon line is a fraction e^{-S} of the integrated intensity over the zero-phonon and multiphonon spectrum.²³ Values of S calculated by this method are collected in Table III and selected values from this table appear in Table I. These two S values in Table I are both only half the best-fit values, another indication that the fitting procedure is oversimplified.

B. Broad Features in Emission Spectra

In this section we will speculate on the origin of the broad features present in the emission spectra of O_2^- in KCl and the three rubidium halides. We are not referring to the low-frequency peaks which we have attributed to librational motion of O_2^- , nor to the "extra" line in $KBr:O_2^-$, which is due to O_2^- with different symmetry. By this definition, then, we notice that no broad features are present in the three alkali halides where O_2^- has trigonal symmetry, NaCl, KBr, and KI.

We propose that these broad features are due to transitions to a ground-state level with a very short lifetime. In KCl this lifetime is not so short as in the rubidium halides, so that a zero-phonon line can still be seen (Fig. 2) together with a multiphonon sideband with much reduced detail. Such a spectrum can be produced by convoluting the main spectrum with a broadening function about 20 cm^{-1} wide. In the rubidium halides the lifetime is shorter, and the consequent greater broadening causes the zero-phonon line to disappear into the

TABLE III. Coupling coefficients, determined by integration of emission intensities, 2°K.

v''	4	5	6	7	8	9	10	11	12
KBr: O_2^-	1.16	1.01	0.94	0.80	0.72	0.72	0.66	0.60	0.55
KI: O_2^-	0.88	0.67	0.52	0.47	0.42	0.38	0.29

TABLE IV. Calculated shift of the broad features in the O_2^- emission, compared with experimental values, in cm^{-1} .

Crystal	λ/Δ^a	Δ	$\omega_e'' - \Delta^b$	Observed shift
KCl	0.231	650	450	460
RbCl	0.135	1100	0	0
RbBr	0.169	890	210	230
RbI	0.190	790	310	320

^aFrom Ref. 4.

^b ω_e'' value approximately 1100 cm^{-1} , see Ref. 5.

noise and all details to be erased from the multiphonon sideband. We can measure the frequency displacement of the broad feature from the ordinary emission at a given quantum number v'' by measurement of the broad (multiphonon) maximum relative to the peak of the normal multiphonon sideband. For example, in RbCl (Fig. 5) this displacement is approximately zero, since the peak of the broad features is hidden under the normal spectrum, whereas in the RbBr (Fig. 6), the displacement is approximately 230 cm^{-1} . In this manner the four frequency differences shown in Table IV were measured.

We further speculate that the short-lifetime state is one of the ${}^2\Pi_g$ levels of O_2^- split by the D_{2h} crystal field. The ground-state splitting Δ can be calculated from values of λ/Δ obtained from electron-spin-resonance experiments²⁴ if the spin-orbit coupling constant is known; in the following calculations we used the value $\lambda = 150$ cm^{-1} appropriate to atomic oxygen. If the emission transition is from a single excited-state level, and transitions are allowed from this level to both the split ground states, then the broad features could be due to transitions to a transitory upper split level in the ground state. To a first approximation the frequency displacement from the normal spectrum will be $\omega_e'' - \Delta$, if Δ is never greater than ω_e'' . The calculations in Table IV show that this expectation is in good agreement with experiment. There are no broad features in the trigonal cases NaCl, KBr, and KI.

ACKNOWLEDGMENTS

The authors gratefully acknowledge the help of H. Labbé, who prepared all the specimens, F. D. Blair and B. A. Kettles for programming and data processing, and F. R. Lipsett for the use of the luminescence apparatus. One of the authors (M. I.) wishes to thank Dr. J. H. Simpson and the members of the Solid State Group for the hospitality showed to him during his stay at the National Research Council. One of the authors (T. T.) thanks A. J. Sievers and the whole far-infrared group at Cornell University for their generous help.

*National Research Council Postdoctorate Fellow, 1969–1971. Present address: Department of Physics, Tohoku University, Sendai, Japan.

†Work supported in part by the Advanced Projects Research Agency through the Materials Science Center at Cornell University. Present address: Department of Physics, McMaster University, Hamilton, Ontario, Canada.

¹W. Känzig and M. H. Cohen, *Phys. Rev. Letters* **3**, 509 (1959).

²W. Honrath, *Ann. Physik*, **29**, 421 (1937).

³J. Rolfe, F. R. Lipsett, and W. J. King, *Phys. Rev.* **123**, 447 (1961).

⁴H. R. Zeller and W. Känzig, *Helv. Phys. Acta* **40**, 845 (1967).

⁵M. Ikezawa and J. Rolfe, *J. Chem. Phys.* (to be published).

⁶L. A. Rebane, *Trudy I.F.A.A.N. Est. S.S.R.* **37**, 45 (1968).

⁷L. A. Rebane and P. M. Saari, *Fiz. Tverd. Tela* **12**, 1945 (1970) [*Sov. Phys. Solid State* **12**, 1547 (1971)].

⁸L. A. Rebane, O. I. Sild, and T. J. Haldre, *Izv. Akad. Nauk S.S.R.* **35**, 1396 (1971).

⁹W. E. Bron, *Phys. Rev.* **140**, A2005 (1965).

¹⁰T. Timusk and M. V. Klein, *Phys. Rev.* **141**, 664 (1966).

¹¹A. A. Maradudin, *Solid State Phys.* **18**, 274 (1966).

¹²M. V. Klein, *Phys. Rev.* **131**, 1500 (1963).

¹³M. Wagner, *J. Chem. Phys.* **41**, 3939 (1961).

¹⁴Off-diagonal elements of S_{ij} are nonzero, for example, between E_g and A_{1g} in the presence of an orthorhombic

distortion, since G_{ij} is no longer diagonal in these coordinates.

¹⁵T. Gethins, T. Timusk, and E. J. Woll, Jr., *Phys. Rev.* **157**, 744 (1967).

¹⁶R. A. Cowley, W. Cochran, B. N. Brockhouse, and A. D. B. Woods, *Phys. Rev.* **131**, 1030 (1963).

¹⁷G. Herzberg and E. Teller, *Z. Phys. Chem.* **B21**, 410 (1933).

¹⁸The final state relevant to the Herzberg–Teller selection rules is the state towards which the system *initially* relaxes. In a harmonic system the modes are independent and each relaxes towards its equilibrium position. In an anharmonic system this is not the case and the system may not relax towards the vibrational ground state. In terms of the notation of the previous section the system relaxes in the direction of the vector $\partial E_g / \partial Q_i$, the gradient of the potential surface, which is not the same as $Q_{0i} = \sum_l \langle Q | l \rangle q_{0l}$, the vector that describes the displacement of the equilibrium position of coordinate Q_i .

¹⁹A. Kiel, *Phys. Rev.* **140**, A606 (1965).

²⁰R. W. Ward and T. Timusk, *Phys. Rev. B* **5**, 2351 (1972).

²¹T. Timusk and M. Buchanan, *Phys. Rev.* **164**, 395 (1967).

²²L. Rebane and T. Saar, *Izv. Akad. Nauk Est. S.S.R.* **15**, 297 (1966).

²³See, for example, D. B. Fitchen, in *Physics of Color Centers*, edited by W. B. Fowler (Academic, New York, 1968), p. 311.

²⁴Reference 4, p. 860.

Effects of Scattering-Induced Dispersion on Phonons: Thermal Conductivity*

D. Walton

Physics Department, McMaster University, Hamilton, Ontario, Canada

(Received 10 April 1972; revised manuscript received 11 September 1972)

It is well known that scattering leads to dispersion. The two constitute, respectively, the imaginary and the real parts of the index of refraction, which are connected by Kramers–Kronig relations. The effects of scattering-induced dispersion on the thermal conductivity have been ignored heretofore. It is shown that for strongly interacting and/or highly concentrated systems the additional dispersion will make a significant difference to the calculated thermal conductivity. The conductivity including dispersion has been calculated and compared with experimental results for solid ^3He - ^4He mixtures, and for the $\text{KCl}:\text{CN}^-$ system. In order to conform to the dispersion relations for the latter, it was necessary to use a model for which the scattering cross section varied as the phonon frequency to the fourth power, in the low-frequency limit. For a multilevel system the scattering cross section must depend on the occupation of the levels. This leads to a temperature dependence of the cross section. Expressions for the cross section appropriate to multilevel systems were derived, and employed in calculating the thermal conductivity of $\text{KCl}:\text{CN}^-$. These expressions are similar to those obtained by numerous investigators for spin systems.

INTRODUCTION

In treating the interaction between long-wavelength phonons and defects, attention has been focussed entirely (except for paramagnetic ions) on the effect on the phonon lifetime. Heretofore, most experimental data bearing on these interac-

tions came from thermal-conductivity measurements. The analysis of the data is usually performed using a relaxation time for the phonons to provide the resistance to heat flow in a crystal which is assumed to be an isotropic Debye solid. This, of course, is the simplest model that can be used and, bearing in mind certain uncertainties